Electronic Supplementary Material (ESI) for Nanoscale.
This journal is © The Royal Society of Chemistry 2014

Supporting Information for

Generation of plasmonic Au nanostructures at visible wavelength using two-dimensional parallel dip-pen nanolithography

Jae-Won Jang,*[a] ByeongChan Park,[a] and Saju Nettikadan[b]

[a] *Department of Physics, Pukyong National University, Busan, 608-737, Korea.*
[b] *Nanofabrication Systems Division, NanoInk Inc., Skokie, IL 60077, USA*

**E-mail: jjang@pknu.ac.kr*

I. Optical microscope images of 2D DPN-fabricated Au fishnet structures

Figure S1(a) shows an image of the entire 2D DPN-fabricated Au fishnet structures. The entire image of the structures was obtained by mosaic function in a Zeiss optical microscope. It definitely indicates that the Au fishnet structures were fabricated in a huge area up to 10 mm × 10 mm. Figure S1(b) and S1(c) are optical microscope images with magnifications of 50X and 200X, respectively.

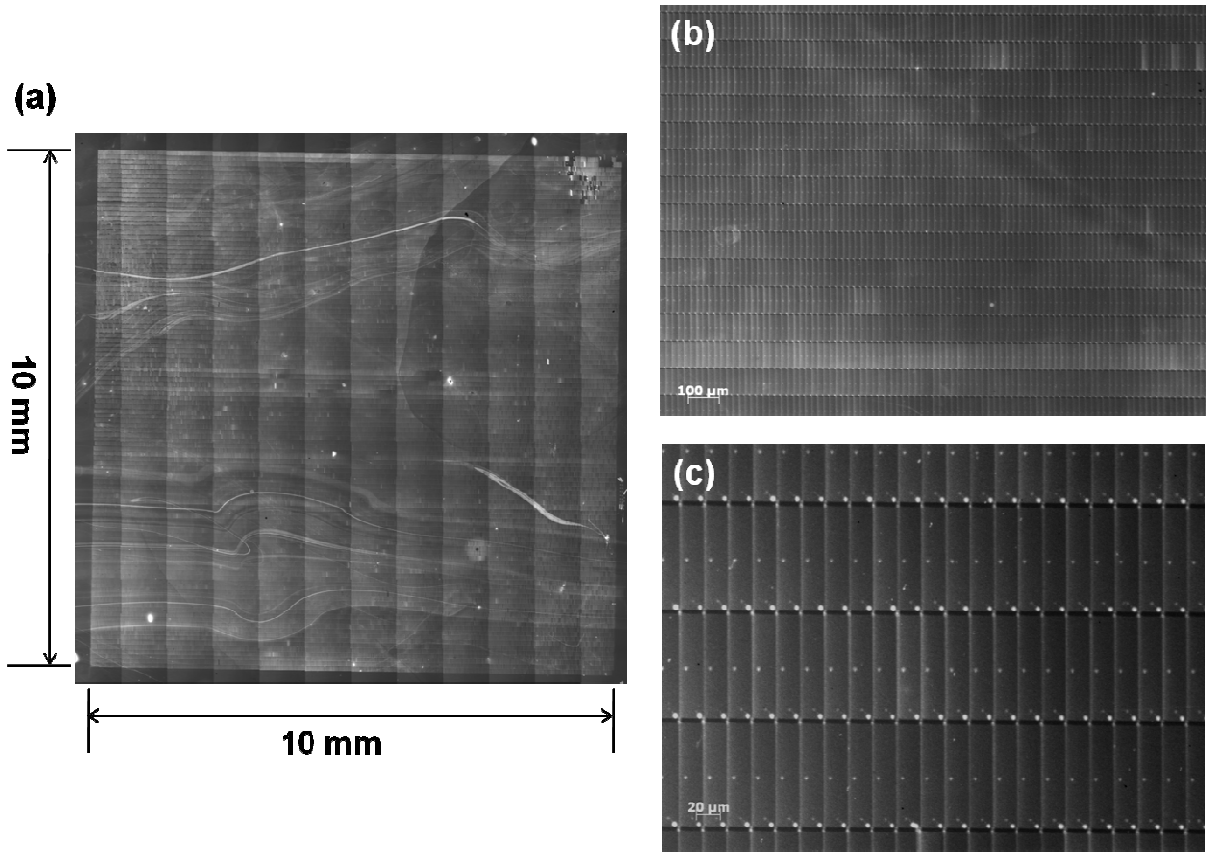

Figure S1 (a) An optical microscope image of the entire Au fishnet structure. (b) 50X and (C) 200X optical microscope images of the Au fishnet structures. The dot patterns in the middle and the edges of the fishnet structure originate from levelling and landing procedures of 2D DPN printing, respectively.

II. High resolution of AFM image and height profiles of Au fishnet structures

Figure S2 shows a 3-dimensional (3D) AFM image of Au fishnet structures and height profiles at the extruded Au line patterns. The perpendicularly crossed two lines show different height profiles (Red and blue colored lines in figure S2). We assume that the non-uniform Au line patterns could be originated from roughness of Au polycrystalline film (in general, 3 ~ 4 nm) and non-uniform wet etching process.

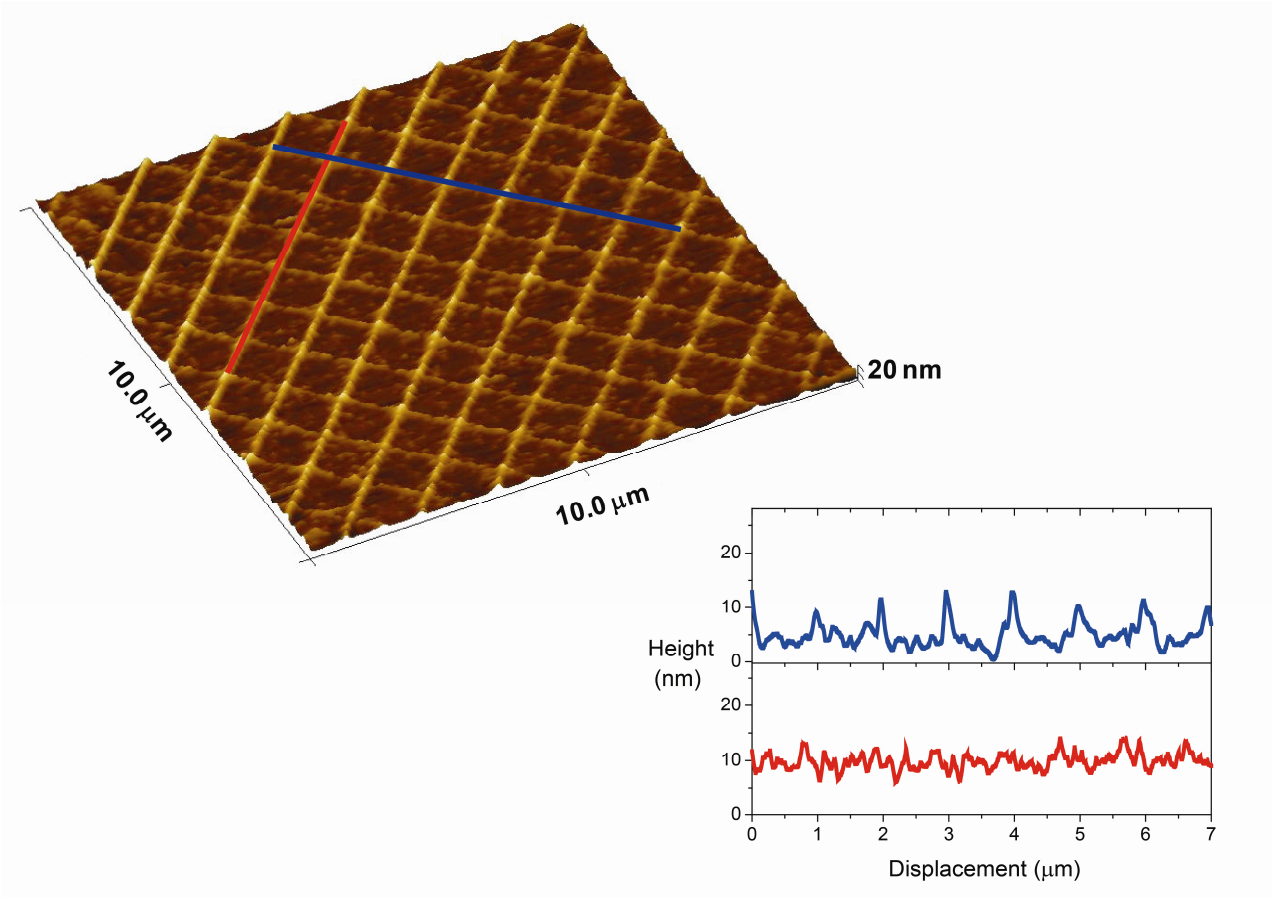

Figure S2 A 3D high-resolution AFM image of Au fishnet structures and height profiles at the extruded Au line patterns. The red and blue colored height profiles are obtained from the red and blue lines in the AFM image, respectively.

III. Fresnel equation for baseline signal fitting

The reflectance of s-polarized light (R_s) can be described by the Fresnel equation as shown in Eq. (S1):

$$R_s = \left| \frac{n_1 \cos\theta_i - n_2\sqrt{1-\left(\frac{n_1}{n_2}\sin\theta_i\right)^2}}{n_1 \cos\theta_i + n_2\sqrt{1-\left(\frac{n_1}{n_2}\sin\theta_i\right)^2}} \right|^2, \qquad \text{(S1)}$$

where θ_i is incidence angle, n_1 and n_2 are the refractive indices at media 1 and 2, respectively. In our system, θ_i is fixed at 70° because of the ellipsometer's experimental condition. Because the experiment was carried out in air, n_1 and n_2 are regarded as 1 and the refractive index of silicon crystal (n_{Si}), respectively. To numerically fit the experimental reflectance spectra in with the Fresnel equation R_s, we consider that n_{Si} is a wavelength dependent function using Eq. (S2)[1, 2]:

$$n_{Si}(\lambda)^2 - 1 = \frac{10.6684293 \cdot \lambda^2}{\lambda^2 - 0.301516485^2} + \frac{0.003043475 \cdot \lambda^2}{\lambda^2 - 1.13475115^2} + \frac{1.5413308 \cdot \lambda^2}{\lambda^2 - 1104.0^2} \ . \qquad \text{(S2)}$$

For fitting in empirical data, the dimensionless coefficient (A), offset (R_0), and wavelength offset (λ_0) are introduced into Eq. (S1), so that Eq. (S3) can finally be obtained.

$$R_s = A \cdot \left| \frac{\cos 70^\circ - n_{Si}(\lambda-\lambda_0)\sqrt{1-\left\{\frac{1}{n_{Si}(\lambda-\lambda_0)}\sin 70^\circ\right\}^2}}{\cos 70^\circ + n_{Si}(\lambda-\lambda_0)\sqrt{1-\left\{\frac{1}{n_{Si}(\lambda-\lambda_0)}\sin 70^\circ\right\}^2}} \right|^2 + R_0 \ . \qquad \text{(S3)}$$

The "Non-Fishnet area" curve in figure 4(a) and 4(b) is well fitted by Eq. (S3) with values 1.0788 (A), -0.39413 (R_0), and 0 nm (λ_0). Whereas, the "Fitting line by Si substrate" curve in figure 4(a) is generated by Eq. (S3) with values 0.27005 (A), 0.22457 (R_0), and 73.27864 nm (λ_0).

[1] *Handbook of Optics, 3rd edition, Vol. 4. McGraw-Hill 2009*

[2] *http://refractiveindex.info*

IV. Au fishnet structure dependent reflectance spectra

Relationship between reflectance spectra and structure of Au fishnet is examined. Figure S3(a) shows finite-difference time-domain (FDTD) simulated reflectance spectra (*s*-polarization) with different line-width (w) and interline distance (d) of Au fishnet structure. It seems that the baseline of spectrum is distorted as “d” and “w” change. In figure S3, an obvious shift of the absorption peak is not obtained; however, the absorption peak seems to be broadened over 500 nm with changing of interline distance.

We practically fabricated Au fishnet structure with 10% of change in interline distance. AFM topography image of the Au fishnet structure with 10% of change in interline distance is represented in figure S3(b). The interline distance is periodically shortened and broadened in both vertical and horizontal extruded Au line patterns. Experimental reflectance spectrum of the Au fishnet structure with 10% of change in interline distance is shown in figure S3(c). Baseline of the reflectance spectrum is quietly distorted over 500 nm, comparing with the spectrum of the original Au fishnet structure (d: 1 μm, w: 100 nm). The change of the ellipsometric reflectance spectrum over 500 nm shown in figure S3(c) is somehow similar with the change of the FDTD simulated spectrum shown in figure S3(a). It may be concluded that plasmonic properties of Au fishnet structure can be controlled in the wavelength region over 500 nm by adjusting structural factor such as interline distance.

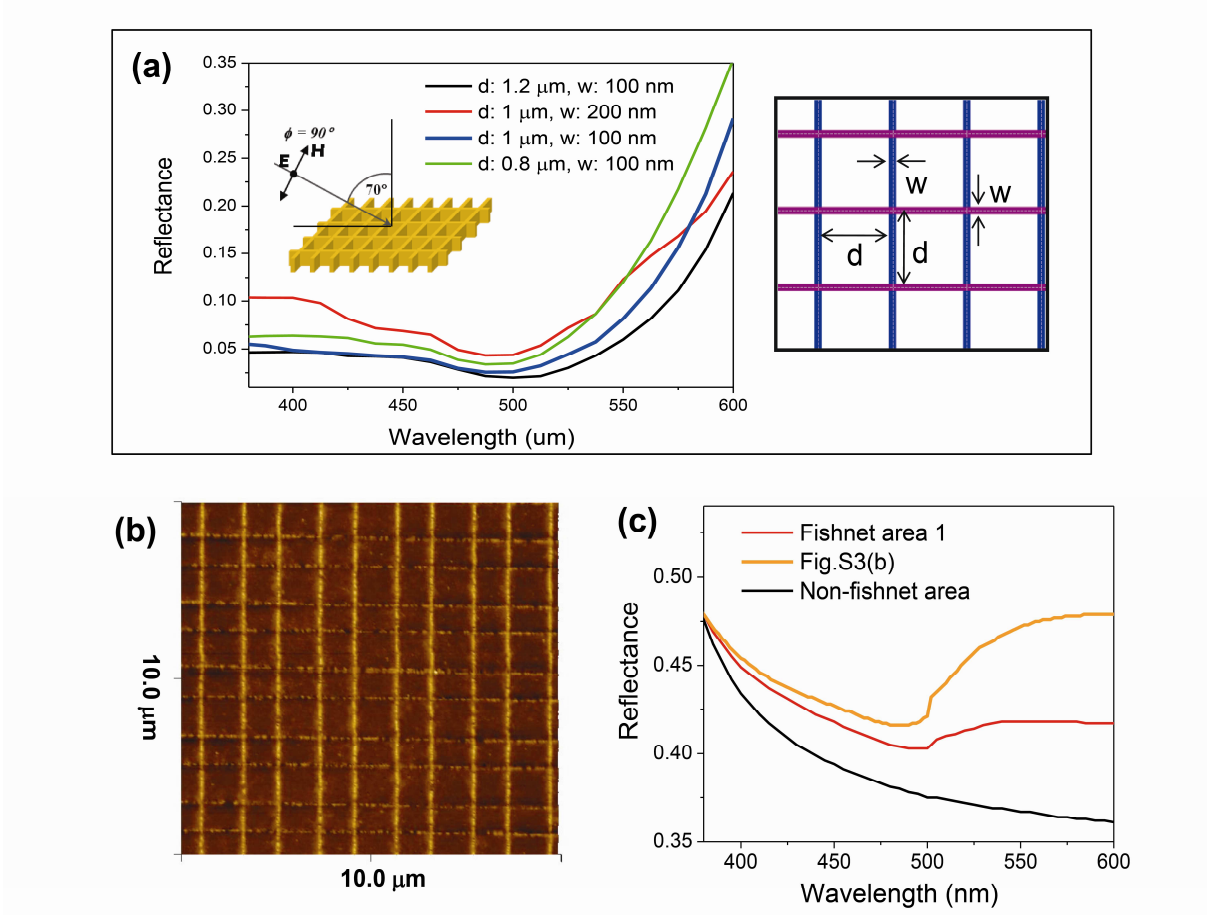

Figure S3 (a) FDTD simulated reflectance spectra with different line-width, "w" and interline distance, "d". Inset shows condition of FDTD simulation, and the scheme at right shows definition of "w" and "d". (b) An AFM topography image of the Au fishnet structure with 1.1 μm and 0.9 μm of "d" and 100 nm of "w". The thickness of extruded Au line patterns is similar as the Au fishnet structure in figure 3. (c) Experimental reflectance spectrum of (b) measured by an ellipsometer is displayed along with the reflectance spectra in figure 4(a).

V. Reflectance spectra of non-patterned Au film with increasing Au etching

Reflectance spectra were measured with non-patterned Au film as Au etching time increases. Thermally deposited Au film (8 nm) with Ti buffer layer (1 nm) on Si(100) substrate was used in this experiments. Reflectance measurements were carried out by an ellipsometer (M2000D, J.A. Woollam Co., Inc.). Au etching was carried out with iron nitrate based aqueous Au etching solution (etching rate: 1 - 2 nm/min). Figure S4 shows Au etching time dependent reflectance spectra of the Au film. The broad absorption peak near 500 nm, which is measured in reflection spectra of the Au fishnet structure, is not shown in figure S4; therefore, it is concluded that Au nanofeatures generated by partial etching (2 min) of Au film do not contribute to the broad absorption peak near 500 nm.

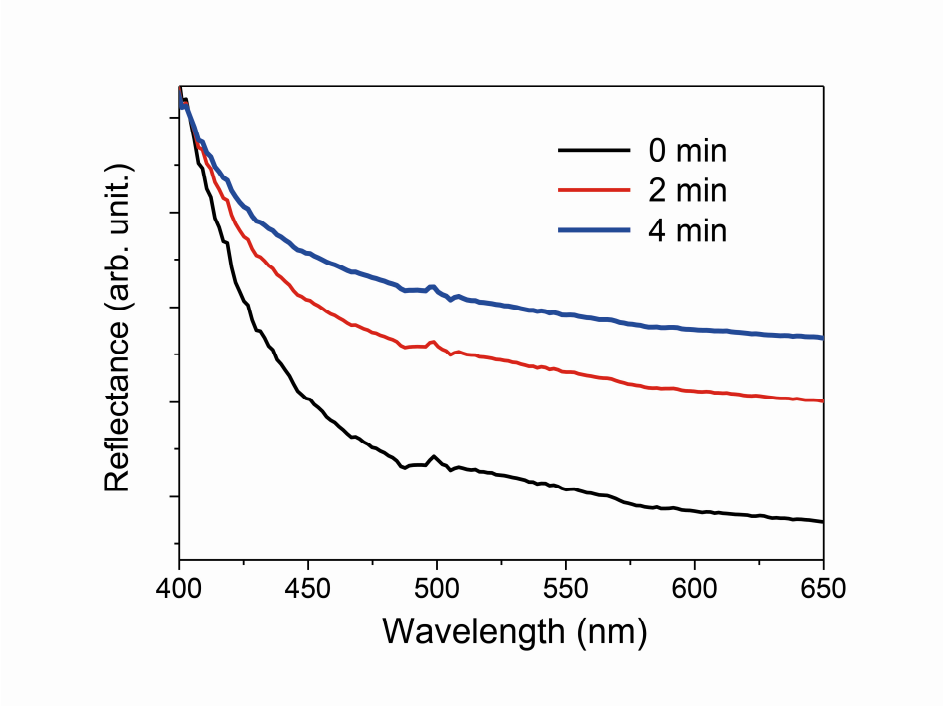

Figure S4 Reflectance spectra of non-patterned Au film dependent on Au etching time of 0 min, 2 min, and 4 min. A broad absorption peak near 500 nm is not shown in all spectra, not similar as the reflectance spectra of Au fishnet structure.

VI. THz metamaterials fabrication by 2D DPN

Using the same 2D DPN fabrication approach, THz metamaterials were also fabricated. 2D DPN-based THz metamaterials were designed with a unit cell of double split-ring resonator (SRR) arrays as shown in figure S6(a). In figure S6(b), the minute dimension of the individual double SRRs is displayed. DPN printings of 1626 dots were carried out to pattern one double SRR. The entire optical microscope image of the THz metamaterials (Au double SRR arrays with 10 nm thickness on a Si substrate) was shown in figure S6(c).

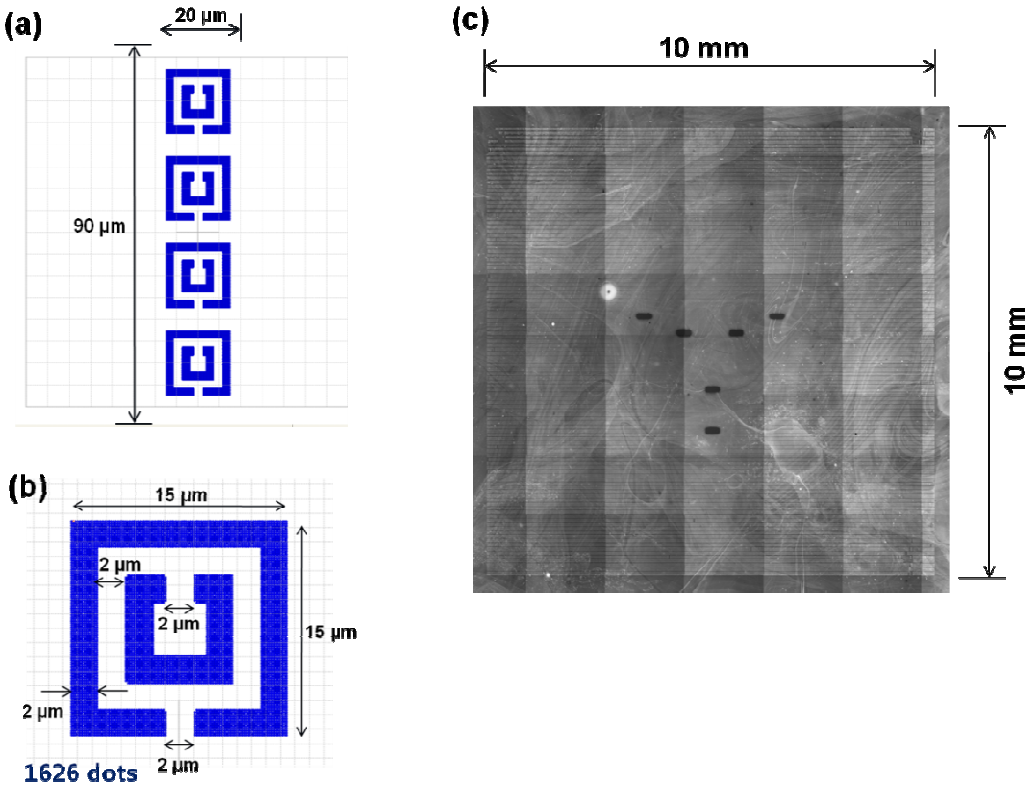

Figure S6 (a) CAD design picture of 2DnPA printing for Au THz metamaterials. (b) Detailed CAD design picture of individual double SRR. (c) An optical microscope image of the entire Au THz metamaterials obtained by the mosaic option of a Zeiss microscope. Y-shaped empty pattern arrays were originated from monitoring windows of 2DnPA.

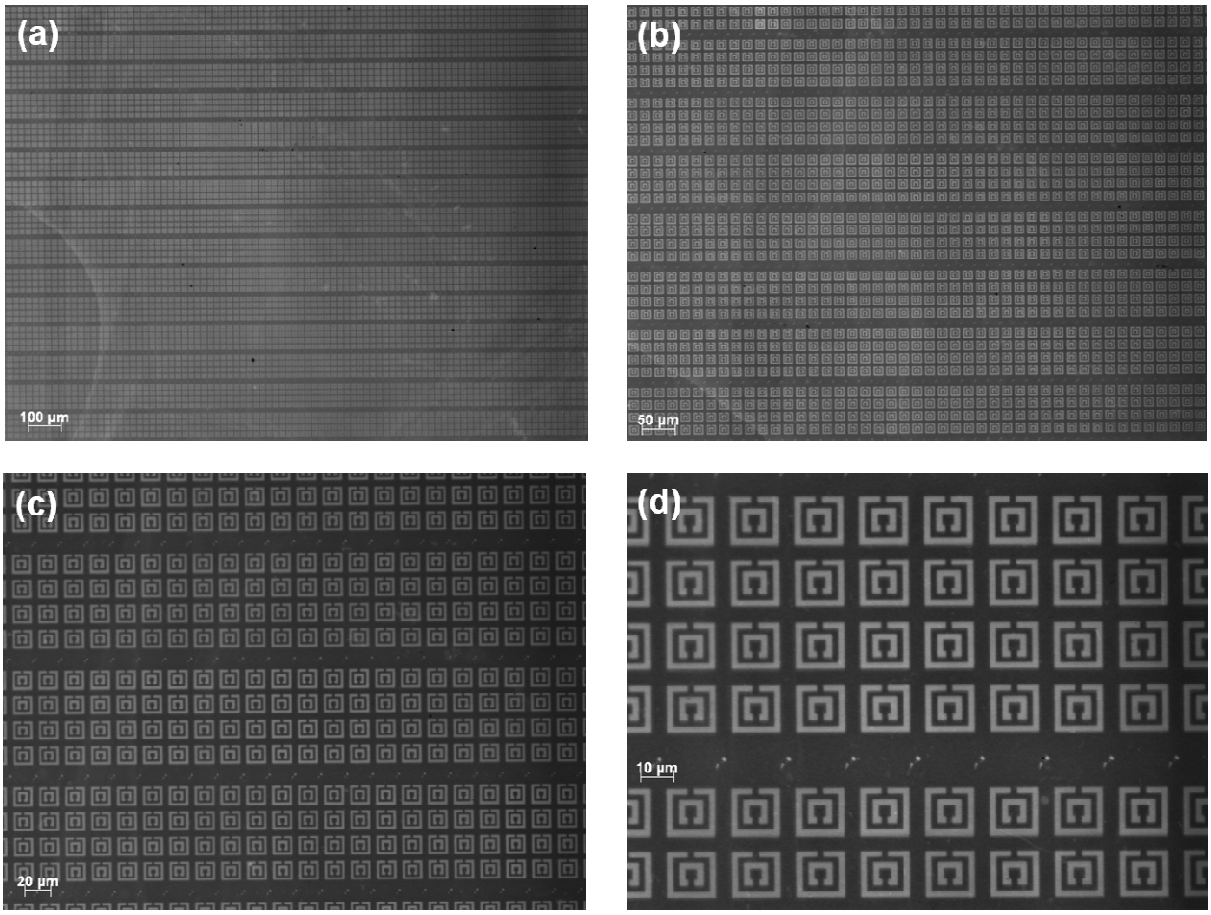

Figure S7 Optical microscope images of the 2D DPN-based THz metamaterials: (a) 50X, (b) 100X, (c) 200X, and (d) 500X. The dot patterns in the areas between the double SRR originate from landing procedures of 2D DPN printing.

VII. Optical property of 2D DPN fabricated THz metamaterials

The optical property of the 2D DPN-fabricated THz metamaterials was measured with the near-IR reflection mapping method (Hyperion 3000 FT-IR, Bruker Optics Inc.) with wavelengths ranging between 2 μm and 11 μm (27–150 THz) as displayed in figure S8. Less near-IR reflection in the split gaps in double SRR structures is shown in figure S8(b). In the results, we can conclude that the 2D DPN fabricated THz metamaterials have a response in the THz region (27–150 THz).

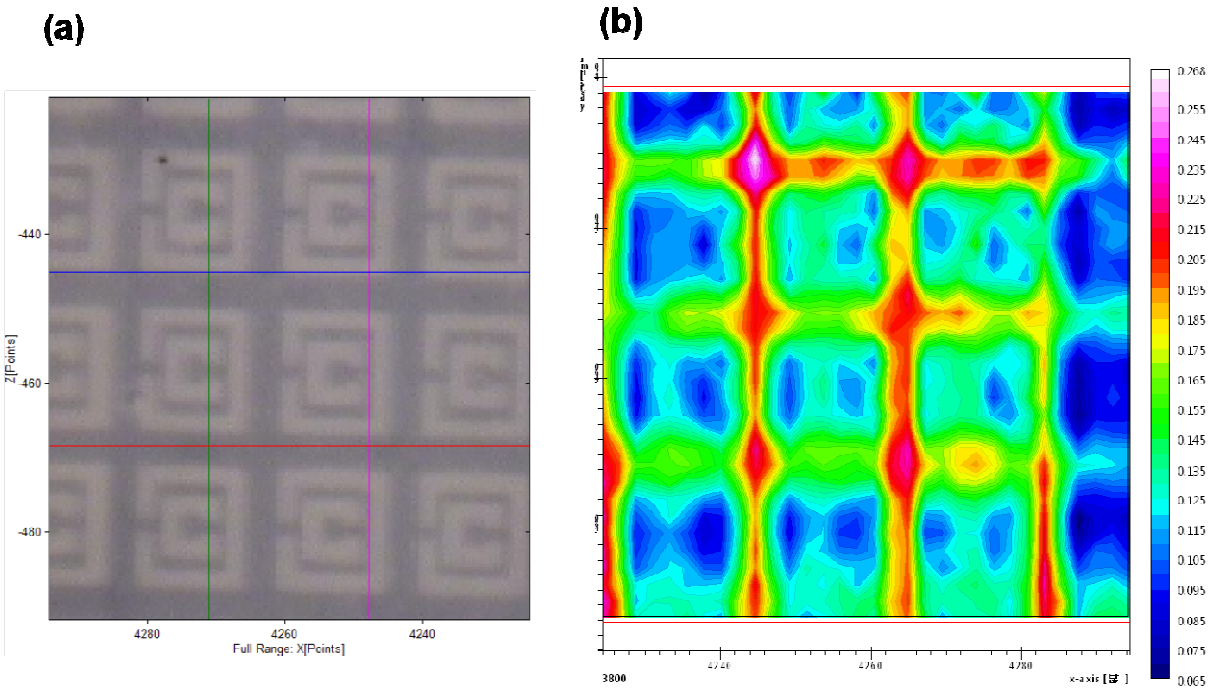

Figure S8 (a) Visible image and (b) near-IR reflection mapping spectrum of the 2D DPN-fabricated THz metamaterials captured by an FT-IR microscope. Blue represents a lower intensity than red in (b).

* *We appreciate Dr. Tom Tague's (at Bruker Optics Inc.) help with the FT-IR measurement.*